JOURNAL OF GEOPHYSICAL RESEARCH, VOL. 89, NO. B12, PAGES 10,125–10,133, NOVEMBER 10, 1984

Noncohesive Critical Coulomb Wedges: An Exact Solution

F. A. DAHLEN

Department of Geological and Geophysical Sciences, Princeton University, New Jersey

Active fold-and-thrust belts or submarine accretionary complexes can be modeled as critically tapered wedges of material on the verge of Coulomb failure everywhere, overlying a basal decollement where frictional sliding is occurring. Ignoring cohesion, the four strength parameters needed to describe a critical Coulomb wedge are its internal and basal coefficients of friction μ and μ_b and its internal and basal Hubbert-Rubey fluid pressure ratios λ and λ_b. An exact relation between surface slope α and basal dip β of a noncohesive critical wedge with uniform properties is derived. The state of stress within such a wedge has the same orientation everywhere, and α is constant if β is, and vice versa. A coefficient of internal friction $\mu = 1.1$ is consistent with the known surface slope, basal dip, and pore fluid pressures in the active fold-and-thrust belt of western Taiwan, assuming that Byerlee's law, $\mu_b = 0.85$, is valid on the base. The wide variety of tectonic styles observed to occur along convergent margins, including subduction erosion, active accretion, subduction without accretion, and even extension and normal faulting, may be controlled by relatively small spatial or temporal variations in either μ_b or λ_b.

INTRODUCTION

This is the third in a series of papers in which fold-and-thrust belts and accretionary wedges along compressive plate boundaries are considered to be analogous to the wedges of deforming soil or snow that form in front of moving bulldozers. The essential premise is that an actively accreting wedge attains a critical taper, which corresponds to an internal state of stress on the verge of Coulomb failure everywhere. The shape of the critical taper is controlled by the coefficient of friction on the basal decollement and by the strength of the rocks composing the wedge: Increasing the basal friction increases the taper, whereas increasing the strength of the rocks decreases it. The geological relevance of this critical Coulomb wedge model is established by *Davis et al.* [1983], hereafter referred to as wedge I. In their paper a simplified version of the essential theory, which ignores the presence of cohesion within the wedge, is described. A more systematic treatment, taking cohesion into account, is presented by *Dahlen et al.* [1984], hereafter called wedge II.

Both wedge I and wedge II make use of a small-angle approximation applicable only to wedges of narrow taper. In this paper it will be shown that, in fact, the case of a noncohesive wedge of arbitrary taper is amenable to a remarkably simple exact analytical solution. By comparing this exact solution with the results obtained earlier, it is shown that the small-angle approximation is rigorously justified in the absence of cohesion for all thin-skinned wedges of geological interest. Although the exact solution cannot be extended to deal with a cohesive wedge, the small-angle approximation should be valid in that case as well, by implication. This justification of the cohesive narrow-taper analysis in wedge II belongs logically in wedge I, but unfortunately, it was only discovered in retrospect.

THEORY

Consider a submarine wedge with a planar upper surface that slopes at an angle α. Let ρ denote the density of the wedge material, and let ρ_w be the constant density of the overlying water. The case of a subaerial wedge can always be recovered by setting $\rho_w = 0$ as in wedge I and wedge II. The exact result takes its simplest form in a system of Cartesian coordinates x, z aligned with the upper surface of the wedge, as shown in Figure 1. The equations of static equilibrium expressed in those coordinates are

$$\frac{\partial \sigma_x}{\partial x} + \frac{\partial \tau_{xz}}{\partial z} - \rho g \sin \alpha = 0 \tag{1a}$$

$$\frac{\partial \tau_{xz}}{\partial x} + \frac{\partial \sigma_z}{\partial z} + \rho g \cos \alpha = 0 \tag{1b}$$

where g is the constant acceleration of gravity. The boundary conditions on the upper surface of the wedge, $z = 0$, are

$$\tau_{xz} = 0 \qquad \sigma_z = -\rho_w g D \tag{2}$$

where D is the local water depth as shown.

Let σ_1 and σ_3 denote the maximum and minimum principal stresses, and let ψ be the angle between σ_1 and the x axis at any point in the wedge. The state of stress in a wedge lacking cohesion and on the verge of Coulomb failure must satisfy the local conditions

$$\tfrac{1}{2}(\sigma_z - \sigma_x) = \frac{-\bar{\sigma}_z}{\csc \varphi \sec 2\psi - 1} \tag{3a}$$

$$\tau_{xz} = \frac{-\tan 2\psi \, \bar{\sigma}_z}{\csc \varphi \sec 2\psi - 1} \tag{3b}$$

where $\mu = \tan \varphi$ is the coefficient of internal friction. The quantity $\bar{\sigma}_z$ is the effective stress:

$$\bar{\sigma}_z = \sigma_z + p_f \tag{4}$$

where p_f is the pore fluid pressure. Since $p_f = \rho_w g D$ on $z = 0$, boundary conditions (2) may be rewritten in terms of the effective stress as

$$\tau_{xz} = \bar{\sigma}_z = 0 \tag{5}$$

As in wedge I and wedge II, it is convenient to introduce generalized Hubbert-Rubey fluid pressure ratio λ, defined by

$$\lambda = \frac{p_f - \rho_w g D}{|\sigma_z| - \rho_w g D} \tag{6}$$

Attention will henceforth be restricted to a wedge with uniform properties, i.e., one for which ρ, μ, and λ are constant.

Paper number 4B0880.
0148-0227/84/004B-0880$05.00

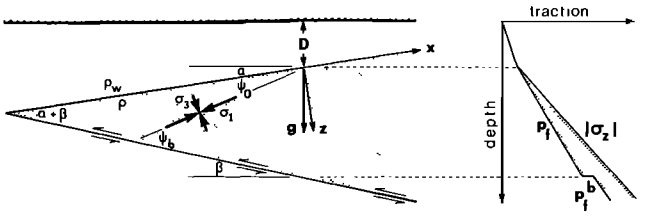

Fig. 1. Cross-sectional sketch of a submarine noncohesive critical wedge showing the Cartesian coordinates x, z and the angles α, β, ψ_0, and ψ_b. Strength in the wedge is proportional to the effective stress $\bar{\sigma}_z$, shown schematically by the shaded area on the right.

In general, as illustrated in wedge II, the orientation of the principal stresses can be expected to vary from place to place within a critical Coulomb wedge. We will now show, however, that if the wedge is uniform and noncohesive, the orientation is everywhere the same, i.e.; $\psi = \psi_0$, a constant. It is this simplifying feature that makes an exact treatment of the problem possible. In fact, it is easily verified by substitution that equations (1), (3), and (5) are satisfied by

$$\bar{\sigma}_z = -(1 - \lambda)\rho g z \cos \alpha \tag{7a}$$

$$\tau_{xz} = (\rho - \rho_w) g z \sin \alpha \tag{7b}$$

provided

$$\frac{\tan 2\psi_0}{\csc \varphi \sec 2\psi_0 - 1} = \left(\frac{1 - \rho_w/\rho}{1 - \lambda}\right) \tan \alpha \tag{8}$$

Equation (8), which gives the stress orientation angle ψ_0 implicitly in terms of α, can alternatively be written in the explicit form

$$\psi_0 = \tfrac{1}{2}\arcsin\left(\frac{\sin \alpha'}{\sin \varphi}\right) - \tfrac{1}{2}\alpha' \tag{9}$$

where α' is a modified slope angle defined by

$$\alpha' = \arctan\left[\left(\frac{1 - \rho_w/\rho}{1 - \lambda}\right) \tan \alpha\right] \tag{10}$$

If a wedge is both dry and subaerial, so that $\lambda = 0$ and $\rho_w = 0$, then $\alpha' = \alpha$. In verifying that the effective state of stress is given by (7), use has been made of the relation $dD/dx = -\sin \alpha$.

Having established that a state of stress characterized by $\psi = \psi_0$ is consistent with the equilibrium equations, the failure criterion, and the upper boundary conditions, all that remains is to examine the conditions on the base. The traction τ_b acting to resist basal sliding is assumed to be governed by a coefficient of friction $\mu_b = \tan \varphi_b$ and a basal pore fluid pressure $p_f{}^b$, i.e.;

$$\tau_b = -\mu_b(\sigma_n + p_f{}^b) \tag{11}$$

where σ_n is the basal normal traction. Both μ_b and the basal fluid pressure ratio defined by

$$\lambda_b = \frac{p_f{}^b - \rho_w g D}{|\sigma_z| - \rho_w g D} \tag{12}$$

are assumed to be constant. The introduction of two separate parameters λ and λ_b allows for the possibility that the pore fluid pressure may experience a sudden change across the basal decollement, as shown in Figure 1. If an effective coefficient of basal friction, $\mu_b' = \tan \varphi_b'$, is defined by

$$\mu_b' = \mu_b\left(\frac{1 - \lambda_b}{1 - \lambda}\right) \tag{13}$$

basal boundary condition (11) may be rewritten more succinctly as

$$\tau_b = -\mu_b'\bar{\sigma}_n \tag{14}$$

where $\bar{\sigma}_n = \sigma_n + p_f$ is the effective stress just above the basal decollement. In general, for a critical wedge to exist, its base must be a zone of weakness or at least no stronger than the interior, i.e.,

$$0 \le \mu_b' \le \mu \tag{15}$$

Let β denote the dip of the basal decollement. The effective basal tractions can be expressed in the adopted x, z coordinate system as

$$\tau_b = \tfrac{1}{2}(\sigma_z - \sigma_x) \sin 2(\alpha + \beta) + \tau_{xz} \cos 2(\alpha + \beta) \tag{16a}$$

$$\bar{\sigma}_n = \bar{\sigma}_z - \tau_{xz} \sin 2(\alpha + \beta) - \tfrac{1}{2}(\sigma_z - \sigma_x)[1 - \cos 2(\alpha + \beta)] \tag{16b}$$

When equations (16) are inserted into boundary condition (14), it is found that the latter is equivalent to

$$\alpha + \beta = \psi_b - \psi_0 \tag{17}$$

where

$$\frac{\tan 2\psi_b}{\csc \varphi \sec 2\psi_b - 1} = \mu_b' \tag{18}$$

Equation (18), which defines angle ψ_b implicitly, may alternatively be written in the explicit form

$$\psi_b = \tfrac{1}{2}\arcsin\left(\frac{\sin \varphi_b'}{\sin \varphi}\right) - \tfrac{1}{2}\varphi_b' \tag{19}$$

Equation (17) is the exact critical taper equation for a noncohesive Coulomb wedge. It defines basal dip β for a wedge of given surface slope α and given properties ρ, μ, λ, μ_b, and λ_b. Note that β is a constant independent of x and z; this was never assumed, nor was it guaranteed at the outset. We began by considering a wedge of constant surface slope α, found the unique state of critical stress (7) within it, and then inferred that a constant decollement dip β was consistent with basal boundary condition (14). Every critical noncohesive wedge with uniform properties thus has a regular triangular cross section with a planar top and bottom and uniformly oriented slip lines within it. The artifice of showing that the constancy of α implies that of β rather than vice versa has been employed only for mathematical convenience. From a physical point of view the decollement dip is a more fundamental quantity, which together with the material properties determines the surface slope.

Critical taper equation (17) has a simple geometrical interpretation, which is illustrated in Figure 1. As shown in wedge I, the quantity ψ_b defined in (19) is the angle between σ_1 and the base. Equation (17) is thus nothing more than the relationship between any two internal angles of a triangle and the opposite external angle.

Insertion of the critical taper equation back into equation (16a) leads to a simple expression for basal shear traction τ_b, namely,

$$\tau_b = (\rho - \rho_w) g z \sin \alpha \left(\frac{\sin 2\psi_b}{\sin 2\psi_0}\right) \tag{20}$$

The term $(\rho - \rho_w)gz \sin \alpha$ has been employed (with $\rho_w = 0$) in glaciology for at least three decades to estimate the traction

acting on the bed of a glacier [*Orowan*, 1949], and it has been used by *Elliott* [1976] to estimate the traction at the base of a wedge-shaped thrust sheet. For a noncohesive wedge on the verge of Coulomb failure everywhere this familiar "glacier formula" must be multiplied by an additional factor $\sin 2\psi_b/\sin 2\psi_0$, as shown by (20).

Because angles α, β, and ψ_0 are all constant, every critical noncohesive wedge is self-similar in the sense that a magnified version of any portion near the toe is indistinguishable from the wedge itself. This property is a consequence of the lack of any inherent length scale in the equations of static equilibrium and the failure equations. A cohesive wedge has on the other hand a natural length scale given by $S_0/\rho g$, where S_0 is the cohesive strength. Because of this a critical cohesive wedge with uniform properties is not self-similar but rather has a surface slope α that increases away from the toe if β is constant. A seemingly peculiar aspect of the state of stress in a noncohesive wedge is the nonalignment of σ_1 and σ_3 with the upper surface. This, however, is allowed since the difference $\sigma_1 - \sigma_3$ actually vanishes along $z = 0$ because the material there is devoid of strength. If there is any cohesion so that the material along the upper surface can sustain a nonzero deviatoric effective stress, then σ_1 and σ_3 must become aligned with the free surface to satisfy the boundary conditions. This alignment is accomplished through the presence of an upper cohesive boundary layer, as discussed in wedge II. The thickness δ of this boundary layer is related to the cohesive length scale by $\delta \sim S_0/[\mu(1 - \lambda)\rho g]$. The variation of ψ within the boundary layer and the consequent curvature of both the slip lines and the surface topographic profile both make it impossible to obtain an exact analytical solution if cohesion is present.

Application to Taiwan and Other Areas

As documented in wedge I, the active fold-and-thrust belt of western Taiwan is characterized by the parameters $\alpha = 2.9° \pm 0.3°$, $\beta = 6° \pm 1°$, and $\lambda = \lambda_b = 0.67 \pm 0.05$. The corresponding theoretical relationship (17) between α and β for various values of μ is shown in Figure 2, assuming that Byerlee's law, $\mu_b = 0.85$, is applicable on the base. The box represents the observed geometry of the Taiwan thrust belt, and the shaded bands correspond to the uncertainty in the measured pore fluid pressure ratio. The best fitting value of the internal friction is $\mu = 1.1$. A slightly lower value was inferred using the approximate theory in wedge I, namely, $\mu = 1.03$. The difference between 1.1 and 1.03 is 6%, which is not an unreasonable error for an approximation that treats a taper of $\alpha + \beta = 8.9°$ as a small angle. The conclusion is unchanged that a higher intrinsic wedge strength is required to satisfy the Taiwan observations if $\mu_b = 0.85$ and $\lambda = \lambda_b$. In wedge II it is shown that cohesion contributes substantially to this higher wedge strength; the value inferred there from the observed step-up angles of forward verging thrust faults, $S_0 =$ 5–20 MPa, is consistent with laboratory measurements of shale and sandstone fracture strengths.

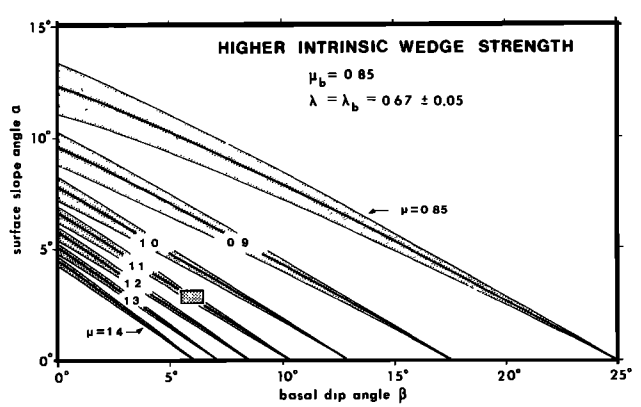

Fig. 2. Surface slope α versus basal dip β for Taiwan pore fluid pressure conditions. Best fitting coefficient of internal friction is $\mu = 1.1$ if $\mu_b = 0.85$.

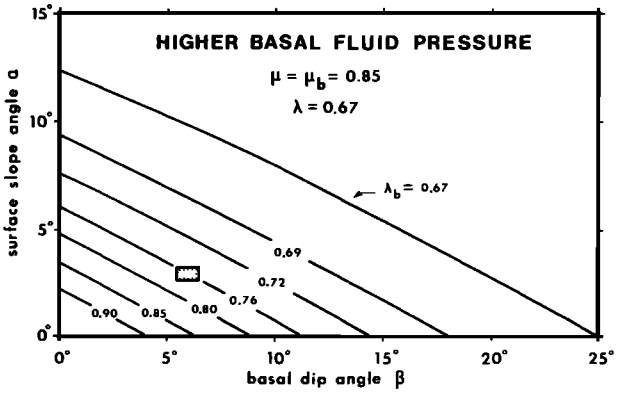

Fig. 3. Possible Taiwan solutions having $\mu = \mu_b$ and a higher pore fluid pressure on the basal decollement.

An alternative to a higher intrinsic wedge strength, which is also consistent with the observed geometry of the wedge in Taiwan, is a higher basal fluid pressure. Since direct fluid pressure information from wells intersecting the basal decollement is only available in the foothills very near the deformation front, this possibility cannot be completely eliminated. Figure 3 shows the theoretical relation between α and β, assuming that $\mu = \mu_b = 0.85$ and $\lambda = 0.67$ for various values of λ_b; Taiwan is again represented by the box. A value $\lambda_b = 0.76$, which is 16% higher than $\lambda = 0.67$, is seen to be consistent with the data. In this interpretation the Taiwan wedge is fractured so pervasively that frictional sliding governed by Byerlee's law is possible on surfaces of optimum orientation everywhere within it, and the lower strength of the base is due to the increased overpressure.

It is frequently argued that Byerlee's law may not be applicable in modeling large-scale faults or fault zones either because of the presence of clay-rich gouges or possibly for other reasons. Figure 4 shows a number of other possible combinations of μ_b and μ in addition to $\mu_b = 0.85$ and $\mu = 1.1$ that are consistent with the Taiwan wedge geometry, assuming that $\lambda = \lambda_b = 0.67$. As already noted in wedge I and wedge II, the coefficient of basal friction may be as low as $\mu_b = 0.2$.

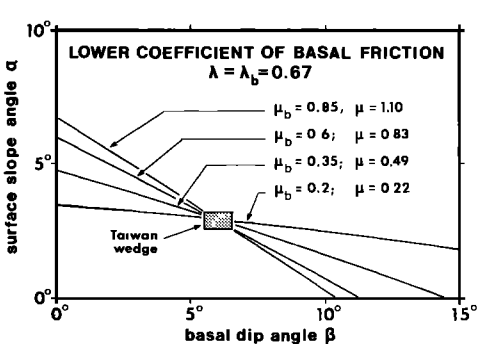

Fig. 4. Possible Taiwan solutions if the assumption is relaxed that Byerlee's law is valid on the decollement. The geometry is consistent with a coefficient of basal friction as low as $\mu_b = 0.2$.

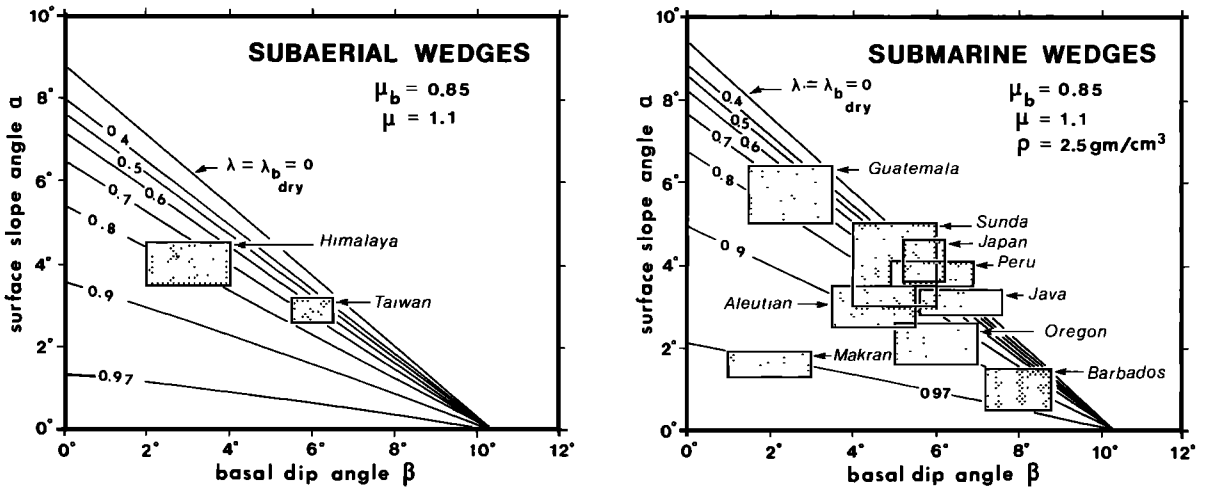

Fig. 5. Surface slope α versus basal dip β for various values of $\lambda = \lambda_b$, using the nominal values of μ and μ_b found in Taiwan. Boxes indicate observed geometries of several active wedges, allowing pore fluid pressure ratios within them to be inferred; the inferred values are all in excess of hydrostatic, $\lambda = \lambda_b = 0.4$.

By adopting the nominal values $\mu_b = 0.85$ and $\mu = 1.1$ found in Taiwan, we can infer the fluid pressure ratios $\lambda = \lambda_b$ for other active accretionary wedges from their observed geometries. The values so inferred are essentially identical to those found earlier using the approximate theory; this is apparent upon comparing Figure 5 with Figure 17 of wedge I. Whereas the approximate theory predicts a linear relationship between α and β for fixed values of the strength parameters, the exact relationship exhibits a slight curvature which is more pronounced when $\mu_b \to \mu$, as seen in Figures 2–5. The theoretically inferred values of $\lambda = \lambda_b$ are all overpressured and in good agreement with nearby fragmentary well data, as noted earlier in wedge I.

The quantity $\sin 2\psi_b / \sin 2\psi_0$, which appears in the formula for basal shear traction τ_b, is plotted versus β for $\mu_b = 0.85$, $\mu = 1.1$, and $\lambda = \lambda_b$ in Figure 6. The inferred value of this parameter for most wedges is considerably in excess of unity; in Taiwan, where the geometry and fluid pressures are best constrained, the best fitting value is $\sin 2\psi_b / \sin 2\psi_0 = 6.7$. Uncritical use of the uncorrected glacier formula to estimate whether τ_b or the apparent coefficient of friction on the basal decollement [*McCarthy et al.*, 1983] will in general lead to values that are biased too low.

Stable Versus Unstable Wedges

There is a simple graphical construction that may be used to determine particular solutions to the exact critical wedge equations (9), (17), and (19). Let $F(\psi)$ denote the function

$$F(\psi) = \frac{\tan 2\psi}{\csc \varphi \sec 2\psi - 1} \tag{21}$$

shown plotted for the case $\mu = 1.1$ in Figure 7. In general, $F(\psi)$ exhibits a maximum and minimum at $\psi = \pm[(\pi/4) - (\varphi/2)]$, where it attains the values $\pm\mu$ as shown. The critical taper $\alpha + \beta$ is given by $\psi_b - \psi_0$, where $F(\psi_b) = \mu_b'$ and $F(\psi_0) = \tan \alpha'$. For every μ_b' in the range $0 \le \mu_b' < \mu$ there are two intersections with $F(\psi)$ and thus two possible values of ψ_b in the range $0 \le \psi_b \le \pi/2$; for $\mu_b' = \mu$ there is a single intersection at the maximum $\psi_b = (\pi/4) - (\varphi/2)$, and for $\mu_b' > \mu$ the wedge existence limit is exceeded, so no solutions are possible. The labels A and B show the correspondence between the intersections of μ_b' with $F(\psi)$ and the intersections of the line having slope μ_b' with the Mohr circle representation of the basal stress state. The complete family of critical tapers $\alpha + \beta$ consists of two distinct branches, one associated with each of the two values of ψ_b; all the solutions discussed in this paper so

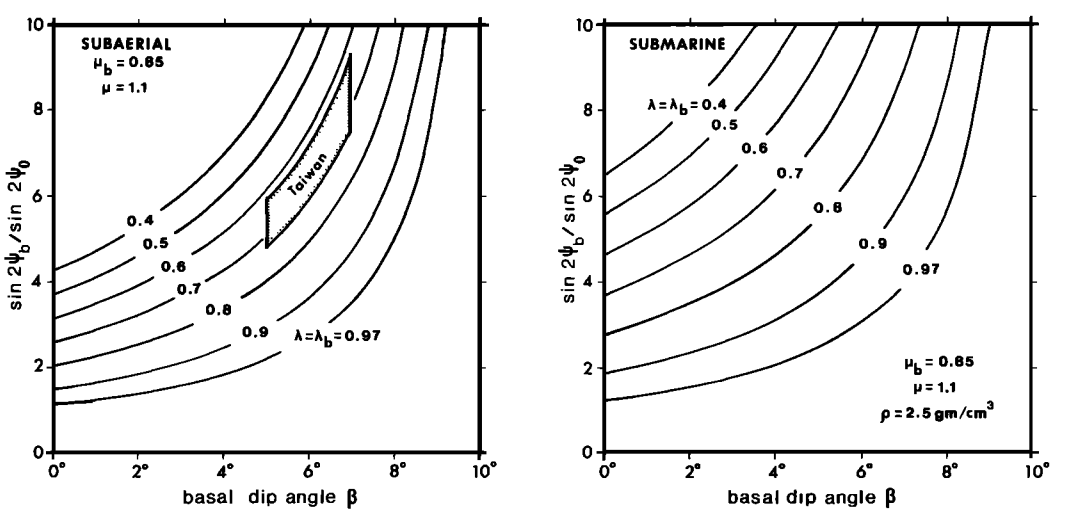

Fig. 6. Plot of the glacier formula correction factor $\sin 2\psi_b / \sin 2\psi_0$ versus β for various values of $\lambda = \lambda_b$. For most of the active wedges shown in Figure 5 the factor lies in the range 3–8.

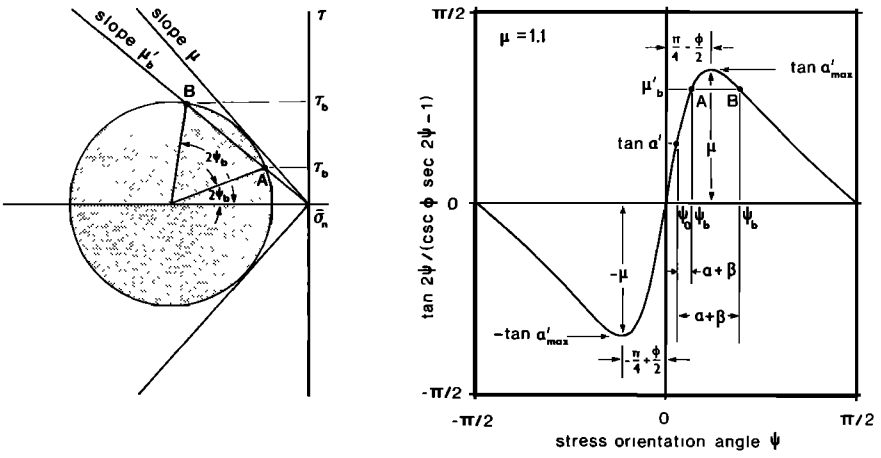

Fig. 7. Mohr diagram illustrating the state of stress at the base of the wedge and graph of $F(\psi)$ showing the angles ψ_0, ψ_b, and $\alpha + \beta$. There are two tapers for every permissible value of tan α', one associated with each of the two possible angles ψ_b.

far have been for the narrower of these two possible tapers, corresponding to intersection A. The existence of two branches of tapers having different basal stress orientations is not entirely unexpected since a similar situation has been noted by *Nye* [1951] in a theoretical discussion of the plastic flow of glaciers.

It is also evident from the graphical construction that there is a maximum possible surface slope, independent of the basal conditions, given by $\alpha_{max}' = \varphi$ or

$$\alpha_{max} = \arctan\left[\frac{\mu(1-\lambda)}{1-\rho_w/\rho}\right] \tag{22}$$

The corresponding value of ψ_0 when $\alpha = \alpha_{max}$ is $\psi_0 = (\pi/4) - (\varphi/2)$. Since failure occurs along surfaces oriented at angles $\pm[(\pi/4) - (\varphi/2)]$ with respect to σ_1, the surface of a maximally steep wedge is a slip face. If the wedge is dry and subaerial, so that $\lambda = 0$ and $\rho_w = 0$, the maximum surface slope angle is the classical angle of repose, $\alpha_{max} = \varphi$. Equation (22) is the generalization of this familiar result to a submarine slope having a nonzero pore fluid pressure p_f.

To illustrate the features just discussed, consider a simple example, having $\rho_w = 0$, $\lambda = \lambda_b = 0$, and $\varphi = 30°$. These parameters are approximate for a subaerial wedge composed of dry sand, as in the laboratory experiments described in wedge I. The theoretical relation between α and β for such a wedge is shown in Figure 8 for various values of the basal friction angle φ_b; all possible solutions having both the surface slope and basal dip positive are represented. The existence of a maximum surface slope at the angle of respose is evident, as is the existence of two branches of tapers for every $\varphi_b < \varphi$. The two branches merge and become identical in the limit $\varphi_b \rightarrow \varphi$. The laboratory experiments described in wedge I were all carried out in a small region of the lower left corner of the plot, roughly along the segment having $\varphi_b = 15°$.

More generally, it is not necessary to restrict the angles α and β to being positive. The only essential restriction is that to be physically meaningful, the taper must be in the range $0 \leq \alpha + \beta \leq \pi$. The complete family of critical dry sand wedges having basal dips $\beta \leq \pi/2$ is shown in Figure 9 for the case $\varphi_b = 10°$. Additional solutions having $\beta > \pi/2$ exist as well, but they are associated with a normal rather than a reverse sense of drag on the basal decollement. Such solutions will not be considered in this paper, although they may be of interest in modeling the low-angle detachment structures in the Basin and Range Province of the western United States [*Wernicke*, 1981; *Allmendinger et al.*, 1983]. Cross sections of

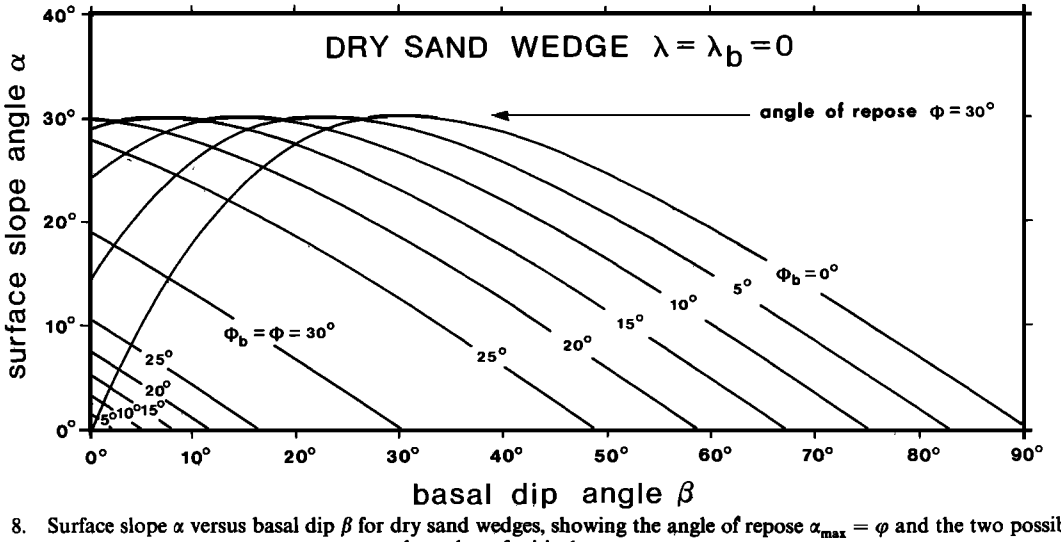

Fig. 8. Surface slope α versus basal dip β for dry sand wedges, showing the angle of repose $\alpha_{max} = \varphi$ and the two possible branches of critical tapers.

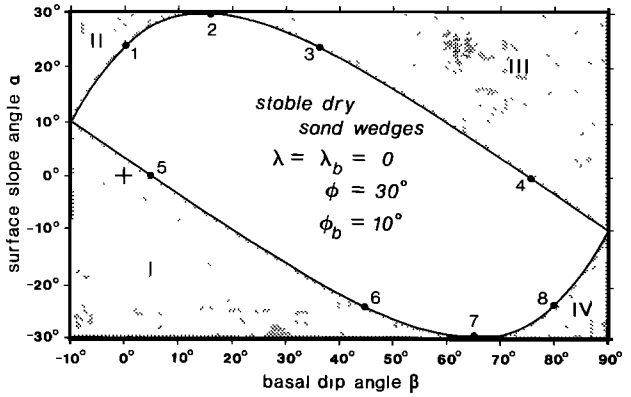

Fig. 9. Diagram showing stable and unstable regions of dry sand wedges having $\varphi = 30°$ and $\varphi_b = 10°$. Critical wedges labeled 1–8 are depicted in Figure 10.

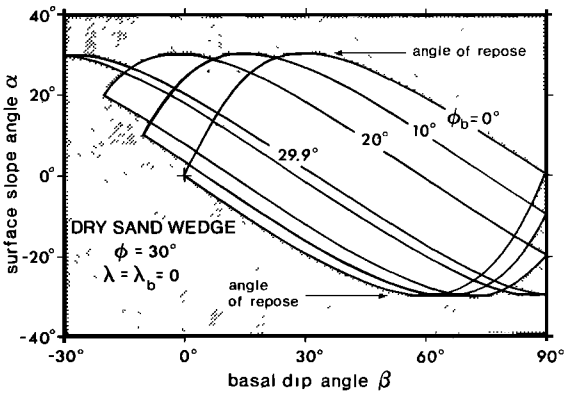

Fig. 11. Stability diagrams for critical dry sand wedges having various basal friction angles, showing shrinking of stable region as φ_b approaches φ.

several critical dry sand wedges at various points on each of the two branches are illustrated in Figure 10; the slip lines which are oriented at $\pm 30°$ to σ_1 are in each case displayed. The locus of critical wedges, by definition, separates wedges that are stable from those that are unstable. The latter occupy the shaded portion of the stability diagram in Figure 9. Wedges in regions I and III fail by thrusting or by a combination of thrusting and normal faulting because the frictional traction on their bases is too great. The resulting deformation acts to increase the taper of wedges in region I and to decrease it in region III. Wedges in regions II and IV are, on the other hand, unstable because the friction on their bases is too weak. They fail in both instances by normal faulting, decreasing their taper in region II and increasing it in region IV. The mode of deformation in region II is gravity spreading, similar to the flow of an accumulating glacier in the direction of its surface slope regardless of the attitude of its base [*Paterson*, 1969]. Any wedge in the unshaded interior portion of the stability diagram is stable as long as the basal friction is unchanged. An increase in the amount of basal friction causes regions I and III to grow in size and regions II and IV to diminish, as illustrated in Figure 11. The stable region shrinks to a narrow sliver and ultimately disappears as the dry wedge existence limit $\mu_b = \mu$ is approached.

EFFECT OF BASAL FRICTION ON TECTONIC STYLE

Recent geophysical investigations and drilling conducted along convergent plate boundaries have revealed a wide variety of tectonic processes at work there. Active accretion and imbricate thrusting, as postulated in early trench slope models

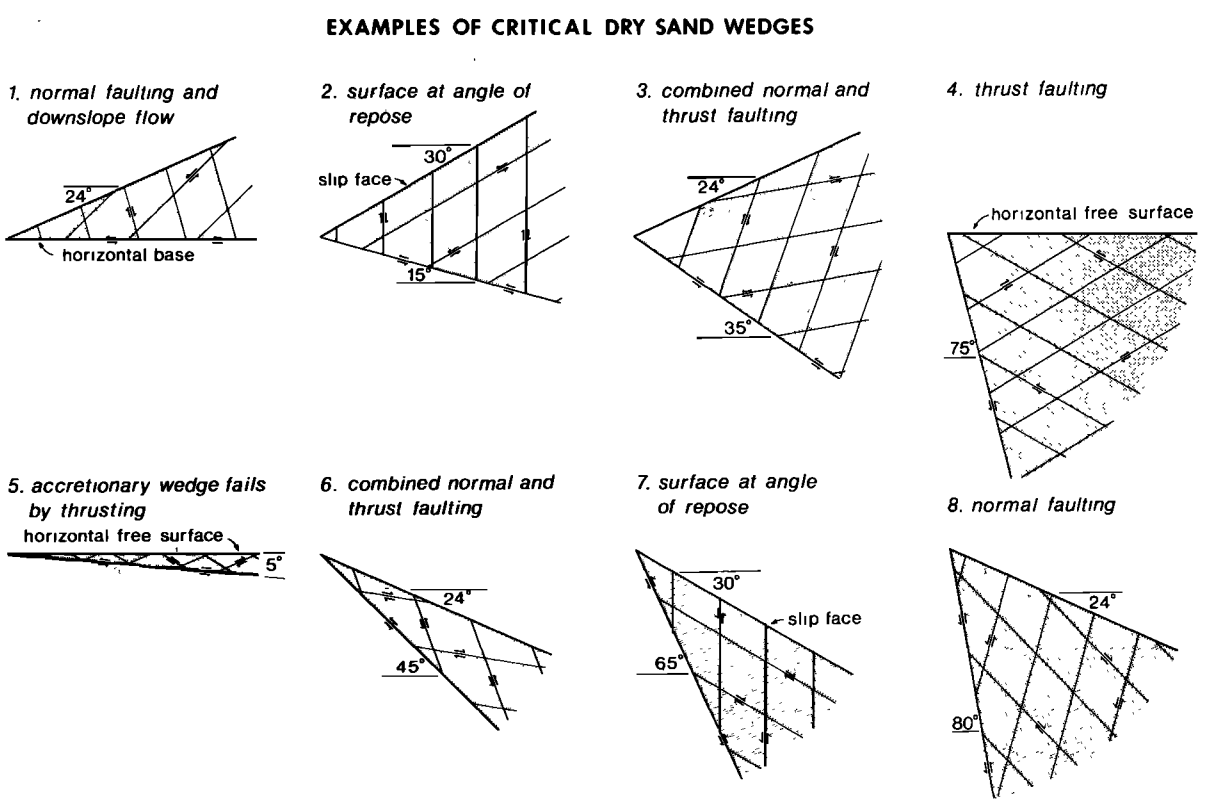

Fig. 10. Cross sections of critical dry sand wedges having $\varphi = 30°$ and $\varphi_b = 10°$. Labels 1–8 correspond to points in stability diagram shown in Figure 9. Angle between slip lines is $90° - \varphi = 60°$.

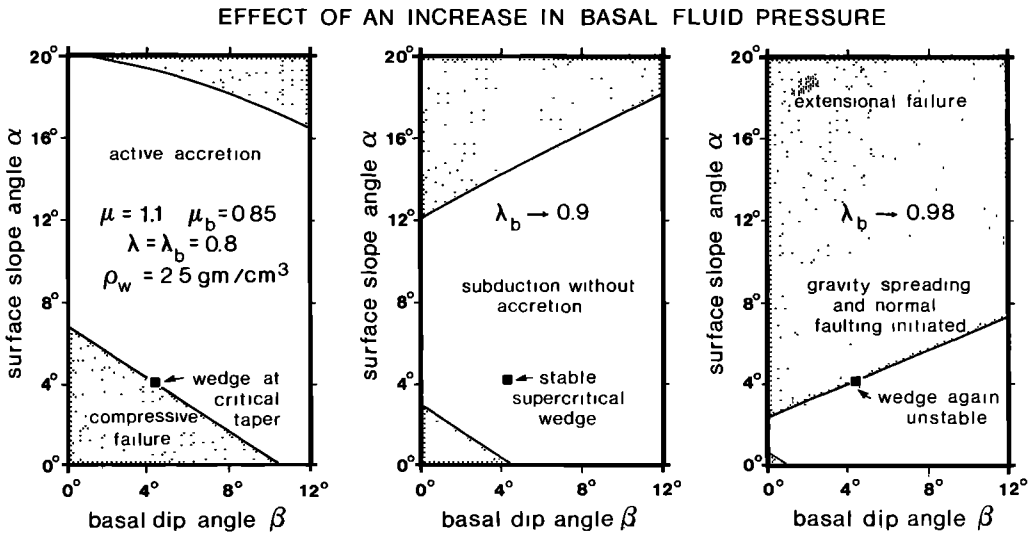

Fig. 12. Surface slope α versus basal dip β for submarine wedges having $\lambda = 0.8$. As λ_b is increased, a hypothetical wedge, shown by squares, first enters the stable regime and then the unstable extensional regime. These three states in the history of the wedge are depicted in Figure 13.

[*Seely et al.*, 1974; *Karig and Sharman*, 1975], are definitely occuring in many regions, such as along the Barbados Ridge [*Westbrook et al.*, 1983; *Moore et al.*, 1982*a*] and off southern Mexico [*Moore et al.*, 1982*b*]. Sediment subduction without accretion is, however, occuring along other margins, such as the Japan Trench [*von Huene et al.*, 1982] and the Mid-America Trench off Guatemala [*von Huene et al.*, 1980]. Normal faults at the base of the inner trench slope and other evidence of extension in the forearc have also been observed in both these localities [*Karig et al.*, 1983; *Aubouin et al.*, 1982]. Finally, subduction erosion, or removal of material from the base of the wedge, has been suggested as the explanation for the observed large-scale Neogene subsidence off Japan [*von Huene et al.*, 1982] as well as for the notable lack of any accreted sediments in the Mariana Trench [*Hussong and Uyeda*, 1981]. It is generally accepted that these variations in the style of tectonism must be the consequence of variations in the degree of frictional coupling between the subducting and overriding plates. The critical Coulomb wedge theory developed here can be used to make this idea more precise. In fact, relatively small variations in the amount of basal friction can easily account for all the variations in behavior that are observed.

This will be illustrated with two hypothetical scenarios, which show what can transpire in the history of a typical overpressured submarine wedge. Initially, the wedge is presumed to be critical and actively accreting, with parameters $\rho = 2.5$ g/cm^3, $\mu_b = 0.85$, $\mu = 1.1$, $\lambda = \lambda_b = 0.8$, $\alpha = 4°$, $\psi_0 = 2.1°$, and $\beta = 4.2°$. Consider the effect of a variation in basal pore fluid pressure ratio λ_b, keeping ρ, μ_b, μ, λ, and β fixed. Such a change might, for example, be produced by a change in the character of the incoming sediments on the subducting plate. A decrease in μ_b will produce the same effect as an increase in λ_b, and vice versa, since theoretically they occur only in the combination $\mu_b(1 - \lambda_b)$. Frequent variations in either λ_b or μ_b are more likely to occur along margins where the rate of subduction of the underlying plate is relatively rapid.

The effect of a reduction in friction due to an increase in λ_b is illustrated in Figures 12 and 13. A moderate increase up to $\lambda_b = 0.9$ reduces the critical surface slope for $\beta = 4.2°$ to near zero, and the wedge becomes supercritical and stable; subduction without accretion can then occur. A more drastic increase up to $\lambda_b = 0.98$ lowers the second critical branch of the stability diagram enough for the wedge to be on the verge of extensional failure. The principal compressive stress σ_1 is in that case nearly vertical, $\psi_0 = 76°$, and steeply dipping normal faults may be initiated as shown. If λ_b continues to increase even further, the wedge will thin and subside by gravity spreading.

Figures 14 and 15 illustrate the opposite effect, that is, of an increase in basal friction due to a decrease in λ_b. A relatively slight decrease down to $\lambda_b = 0.76$ increases the critical taper substantially, leading to increased deformation and steepening of the surface slope. A further decrease down to $\lambda_b = 0.74$ is sufficient to bring the wedge to the verge of the existence limit $\mu_b(1 - \lambda_b) = \mu(1 - \lambda)$. If λ_b decreases beyond this limit, a new decollement must be formed up in the wedge for subduction to

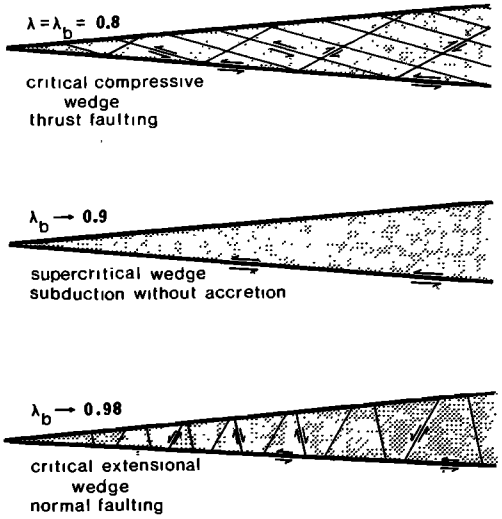

Fig. 13. Cross sections of the hypothetical wedge in Figure 12. The shape of the wedge remains the same, but the tectonic style changes as the basal pore fluid pressure ratio is first raised to $\lambda_b = 0.9$ and then to $\lambda_b = 0.98$. Angle between slip lines is $90° - \varphi = 42.3°$.

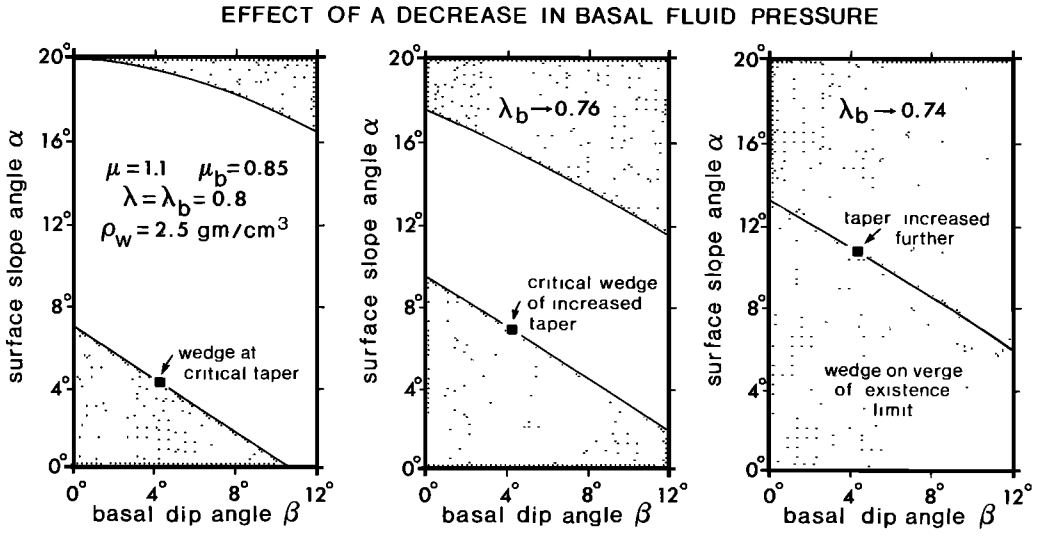

Fig. 14. As λ_b is decreased, a hypothetical wedge increases its critical taper until $\mu_b(1 - \lambda_b) = \mu(1 - \lambda)$, at which point the region of stability vanishes. The three states of the wedge corresponding to the squares are depicted in Figure 15.

continue. One set of slip lines is parallel to the base in a wedge whose basal and interior strengths are equal since $\psi_b = (\pi/4) - (\varphi/2)$, and this will be the preferred attitude of any new decollement. The precise location of the decollement will be governed by preexisting weaknesses, but the net result will always be basal erosion.

In summary, the variations of basal friction required to explain the range of tectonic processes observed along convergent margins are geologically reasonable. The hierarchy of processes going from high friction to low includes subduction erosion, accretion and imbricate thrusting, subduction without accretion, and extension and normal faulting. In the above hypothetical example, variations of the basal pore fluid pressure ratio in the range $\lambda_b = 0.74$–0.98 can account for all of these.

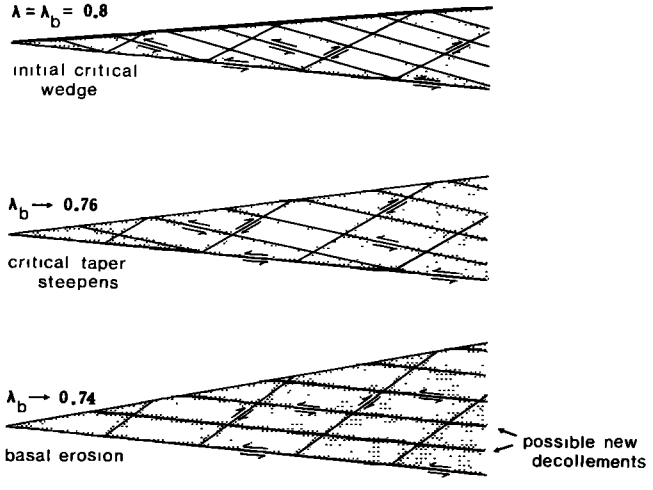

Fig. 15. Cross sections of the steepening hypothetical wedge in Figure 14. When $\mu_b(1 - \lambda_b) = \mu(1 - \lambda)$, a new decollement must be formed, preferentially along one of the slip lines parallel to the base.

Acknowledgments. I thank Dan Davis for repeatedly insisting that a noncohesive wedge must have a triangular cross section because it does not have any natural scale length and John Suppe for his good-humored but futile attempts to teach me some geology. I also thank Glen Stockmal, both for admonishing that the small-angle approximation in wedge II might need additional justification and for calling my attention to the article by Nye. Financial support has been provided by the National Science Foundation under grant EAR-8306157.

REFERENCES

Allmendinger, R. W., J. W. Sharp, D. Von Tish, L. Serpa, L. Brown, S. Kaufman, J. Oliver, and R. B. Smith, Cenozoic and Mesozoic structure of the eastern Basin and Range Province, Utah, from COCORP seismic-reflection data, *Geology, 11*, 532–536, 1983.

Aubouin, J., et al., Leg 84 of the Deep Sea Drilling Project, Subduction without accretion, Middle America Trench off Guatemala, *Nature, 297*, 458–460, 1982.

Dahlen, F. A., J. Suppe, and D. Davis, Mechanics of fold-and-thrust belts and accretionary wedges: Cohesive Coulomb theory, *J. Geophys. Res., 89*, 10087–10101, 1984.

Davis, D., J. Suppe, and F. A. Dahlen, Mechanics of fold-and-thrust belts and accretionary wedges, *J. Geophys. Res., 88*, 1153–1172, 1983.

Elliott, D., The motion of thrust sheets, *J. Geophys. Res., 81*, 949–963, 1976.

Hussong, D. M., and S. Uyeda, Tectonic processes and the history of the Mariana Arc: A synthesis of the results of Deep Sea Drilling Project leg 60, *Initial Rep. Deep Sea Drill. Proj., 60*, 909–929, 1981.

Karig, D. E., and G. F. Sharman, Subduction and accretion at trenches, *Geol. Soc. Am. Bull., 86*, 377–389, 1975.

Karig, D. E., H. Kagami, and DSDP Leg 87 Scientific Party, Varied responses to subduction in Nankai Trough and Japan Trench forearcs, *Nature, 304*, 148–151, 1983.

McCarthy, J., D. W. Scholl, and N. H. Sleep, Accretionary structures along the central Aleutian Trench (abstract), *Eos Trans. AGU, 64*, 870, 1983.

Moore, J. C., J. S. Watkins, T. H. Shipley, K. J. McMillen, S. B. Bachman, and N. Lundberg, Geology and tectonic evolution of a juvenile accretionary terrane along a truncated convergent margin: Synthesis of results from leg 66 of the Deep Sea Drilling Project, southern Mexico, *Geol. Soc. Am. Bull., 93*, 847–861, 1982*a*.

Moore, J. C., et al., Offscraping and underthrusting of sediment at the deformation front of the Barbados Ridge: Deep Sea Drilling Project leg 78A, *Geol. Soc. Am. Bull., 93*, 1065–1077, 1982*b*.

Nye, J. F., The flow of glaciers and ice-sheets as a problem in plasticity, *Proc. R. Soc. London Ser. A, 207*, 554–572, 1951.

Orowan, E., The flow of ice and other solids, *J. Glaciol.*, *1*, 231–240, 1949.

Paterson, W. S. B., *The Physics of Glaciers*, pp. 89–93, Pergamon, New York, 1969.

Seely, D. R., P. R. Vail, and G. G. Walton, Trench slope model, in *The Geology of Continental Margins*, edited by C. A. Burk and C. L. Drake, pp. 249–260, Springer-Verlag, New York, 1974.

von Huene, R., et al., Leg 67: The Deep Sea Drilling Project Mid-America Trench transect off Guatemala, *Geol. Soc. Am. Bull.*, *91*, 421–432, 1980.

von Huene, R., M. Langseth, N. Nasu, and H. Okada, A summary of Cenozoic tectonic history along the IPOD Japan Trench transect, *Geol. Soc. Am. Bull.*, *93*, 829–846, 1982.

Wemicke, B., Low-angle normal faults in the Basin and Range Province: Nappe tectonics in an expanding orogen, *Nature*, *291*, 645–647, 1981.

Westbrook, G. K., and M. J. Smith, Long decollements and mud volcanoes: Evidence from the Barbados Ridge Complex for the role of high pore-fluid pressure in the development of an accretionary complex, *Geology*, *11*, 279–283, 1983.

F. A. Dahlen, Department of Geological and Geophysical Sciences, Guyot Hall, Princeton University, Princeton, NJ 08544.

(Received January 1, 1984;
revised May 25, 1984;
accepted June 15, 1984.)